J Mater Sci (2018) 53:7475–7485

Computation

A comprehensive study of the high-pressure–temperature phase diagram of silicon

Cong Li[1], Cuiping Wang[1], Jiajia Han[1,*], Lihui Yan[1], Bin Deng[1], and Xingjun Liu[1,*]

[1] College of Materials and Fujian Provincial Key Laboratory of Materials Genome, Xiamen University, Xiamen 361005, People's Republic of China

Received: 25 October 2017
Accepted: 29 January 2018
Published online: 6 February 2018

ABSTRACT

A high-pressure–temperature (*P*–*T*) phase diagram of silicon (Si) has been constructed in a range of temperatures covering from 0 to 2000 K and pressures up to 80 GPa. In this system, there is a potential for the following phases to occur: cubic diamond, β-tin, simple hexagonal, double-hexagonal close-packed, hexagonal close-packed and face-centered cubic. Besides, the lattice vibrational energy and thermodynamic quantities of each phase were calculated, in combination with quasi-harmonic approximation using the first-principles phonon density of state. The calculated temperature dependencies of thermodynamic quantities are in good agreement with experimental and theoretical observations. Thereinto, the Gibbs free energy differences of these six phases, as a function of pressure and temperature, were used to define the phase boundaries of the *P*–*T* phase diagram of Si. The results in this work not only integrate previous experimental and theoretical investigations, but also successfully predict the phase relationships of the stable phases of Si under conditions of high temperature and pressure for the first time.

Introduction

Structural phase transitions in semiconductors under high-pressure conditions are a long-standing subject of considerable experimental and theoretical research [1]. In particular, silicon (Si) has become one of the most intensively studied elements, because of the indispensable usages of crystalline or amorphous Si in solid-state electronics and photovoltaic devices [2]. Additionally, Si has critical influence on the properties of the Earth's core [3], which is believed to be composed of iron-dominated alloys, perhaps with Si or Ni as minor components. In this context, Si plays a prominent role in the study of pressure-induced phase transitions of solid elements [4].

It is well known that, under ambient conditions, the most stable phase of Si is the cubic diamond (cd) structure [5]. To date, it has been found that the cd phase can transform into a high-pressure metallic phase, namely β-tin in the range of 10–12 GPa [6–12]. Furthermore, the β-tin structure transforms upon compression at around 13–16 GPa [11] into the simple hexagonal (sh) phase [10]. This sh phase is stable up to about 38 GPa, and it then transforms into

Address correspondence to E-mail: jiajiahan@xmu.edu.cn; lxj@xmu.edu.cn

https://doi.org/10.1007/s10853-018-2087-9

an unidentified phase Si-VI [10, 13] that is assigned to be a double-hexagonal close-packed (dhcp) structure [14–16]. This structure consists of stacked hexagonal close-packed (hcp) and face-centered cubic (fcc) layers. With the increase in pressure, the hcp phase is observed near 42 GPa [10, 13, 14], which in turn transforms to a fcc phase [14] around 79 GPa. The fcc phase is stable up to the highest pressure of about 248 GPa [13]. When the pressure is released, the high-pressure phases transform into a large number of metastable phases such as bc8 [6, 9, 11, 17–29], r8 [20–22], st12 [6, 19], Si-VIII and Si-IX [19, 23] rather than the original phase. However, reports of these metastable phases are not comprehensive.

Although many experimental [5, 7, 10, 11, 14, 19, 24] and theoretical [16, 25–31] reports are available that consider phase transitions of Si in the range of pressure 0–20 GPa, there are no studies on phase transitions at higher pressures and temperatures. Therefore, an integrated P–T phase diagram for Si had not been produced before the present investigation was implemented. To better understand the behavior of Si under the extreme conditions, as well as its role in defining the properties of the Earth's core, it's significant to extend the P–T phase diagram for Si with physical descriptions of the thermodynamic properties.

To this end, theoretical calculations of the main six phases (cd, β-tin, sh, dhcp, hcp and fcc) mentioned above were performed with the help of quasi-harmonic approximation (QHA) in the present investigation, which used the phonon density of states (phDOS) or a mesh of phonon frequencies for each calculated crystal volume. A similar approach was used by Wang et al. [32] and Mei et al. [33] to predict the P–T phase diagrams of cobalt (Co) and titanium (Ti). The present paper is organized as follows: In section "Theory," the theory of Helmholtz energy calculation in QHA is briefly introduced. The computational details of the first-principles calculation are described in "Computational details" section. The results and discussions of the investigation are presented in "Results and discussion" section. Finally, the conclusions of this work are presented in "Conclusions" section.

Theory

The QHA derives from the assumption that the harmonic approximation holds for every value of the crystal volume and then takes into account part of anharmonic effects by varying crystal volume. It is a phonon-based model of crystal lattice vibrations used to describe volume-dependent thermal effects. The Helmholtz energy (F) at volume V and temperature T can be approximated as

$$F(V,T) = E_{\mathrm{sta}}(V) + F_{\mathrm{vib}}(V,T) + F_{\mathrm{ele}}(V,T) + F_{\mathrm{zp}}(V,T), \tag{1}$$

where E_{sta} is the ground-state energy of a static lattice at volume V, F_{vib} is the vibrational energy of the lattice ions, and F_{ele} is the thermal electronic contribution to the free energy, F_{zp} is the zero-point motion energy of the lattice given by

$$Fzp = \frac{1}{2}\sum_{qj}\hbar\omega j. \tag{2}$$

Under QHA, F_{vib} can be calculated from phDOS by

$$F_{\mathrm{vib}} = k_{\mathrm{B}}T\sum_{\mathbf{q}j}\ln\left\{1-\exp\left[\frac{-\hbar\omega_j(\mathbf{q},V)}{k_{\mathrm{B}}T}\right]\right\}, \tag{3}$$

where ω_j is the phonon frequency of the jth mode of wave vector $\mathbf{q}$ in the first Brillouin zone.

We write F_{latt} as

$$Flatt = Fzp + Fvib. \tag{4}$$

It can also be calculated from the phDOS $g(\omega)$ via [34]

$$F_{\mathrm{latt}} = \int\left[\frac{1}{2}\hbar\omega + k_{\mathrm{B}}T\ln\left(2\sinh\frac{\hbar\omega}{2k_{\mathrm{B}}T}\right)\mathrm{d}\omega g(\omega)\right], \tag{5}$$

where k_{B} is the Boltzmann constant. The phDOS is written as

$$g_j(\omega) = V/2\pi^3\int\mathrm{d}\mathbf{q}\delta[\omega-\omega j(\mathbf{q})]. \tag{6}$$

The total DOS is normalized to

$$\int g(\omega)\mathrm{d}\omega = 3nN, \tag{7}$$

where n is the number of atoms in the unit cell and N is the number of the unit cells.

F_{el} can be evaluated by the finite temperature DFT with the help of the Fermi–Dirac smearing [35]. At low temperature, F_{el} is very small and can be neglected, but at high temperature, it probably changes final conclusions.

Computational details

Density functional calculations within the generalized gradient approximation (GGA), as implemented in the Vienna ab initio simulation package (VASP) [36, 37], were utilized to investigate the cd, β-tin, sh, dhcp, hcp and fcc structures of Si in this study. These structural configurations and associated information are shown in Fig. 1. The Perdew–Burke–Ernzerhof GGA (GGA-PBE) [38], for the exchange-correlation potential, was employed for all calculations. Pseudo-atomic calculations were performed for Si s^2p^2. The projector augmented wave (PAW) [39] method was adopted. The total energies were converged to 10^{-6} eV/cell with 400 eV plane wave cutoff energy. The Brillouin zone samplings were performed by the Monkhorst–Pack scheme [40] with a 13 × 13 × 13, 8 × 8 × 14, 13 × 13 × 8, 11 × 11 × 7, 11 × 11 × 7 and 13 × 13 × 13 k-mesh for the cd, β-tin, sh, dhcp, hcp and fcc structures, respectively. The unit cell was used as the initial structure in the process of calculation.

Phonon frequency calculations were carried out for the framework of the supercell approach, using density functional perturbation theory (DFPT) [41], as implemented in the PHONOPY code [42, 43], in which the force constants were calculated using VASP. To maintain the high accuracy, a 2 × 2 × 2, 2 × 2 × 4, 4 × 4 × 4, 4 × 4 × 1, 3 × 3 × 3 and 2 × 2 × 2 supercell consisting of 64, 64, 64, 64, 54 and 32 atoms was adopted for the cd, β-tin, sh, dhcp, hcp and fcc structures, respectively. In the calculations of phonon frequency, the convergences of total energy and the maximum force of ionic relaxation were set to

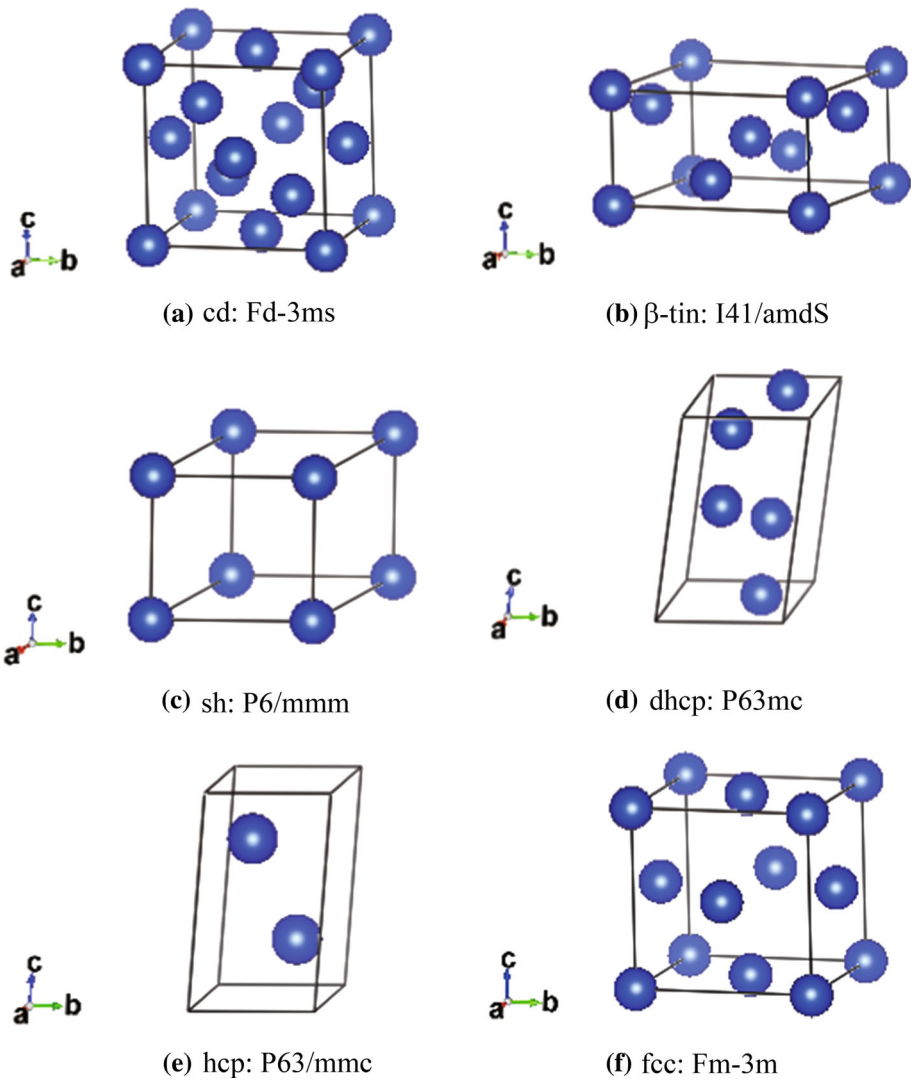

Figure 1 Crystal structures of Si in **a** cd, **b** β-tin, **c** sh, **d** dhcp, **e** hcp and **f** fcc phases.

be less than 10^{-8} eV/atom and 10^{-3} eV/Å. The high-pressure phase boundaries of Si then were automatically depicted by the PHASEGO toolkit [44–46].

Results and discussions

Static energy and structural stability

The total energies of the cd-, β-tin-, sh-, dhcp-, hcp- and fcc-Si phases at different volumes were calculated and fitted by the third-order Birch–Murnaghan (B–M) equation of state (EOS) [47, 48] to obtain the equilibrium properties in the ground state. The total energy for each phase, calculated as a function of volume per atom after fully relaxing the cell under a fixed volume, is presented in Fig. 2a. Apparently, the most stable phase is cd-Si in the ground state, due to its markedly lowest total energy. The equilibrium properties for these six phases, such as the lattice parameter (a), c/a ratio, atomic volume (V_0), isothermal bulk modulus (B_0), first derivative of bulk modulus with respect to pressure (B_0') at 0 K and the atomic energy of equilibrium state (E_0), are all listed in Table 1, where the available experimental data [9, 10, 49] and calculated results [50–52] are included for reference. By comparison, the calculated a, c/a and V_0 of cd, β-tin, sh and hcp phases are numerically consistent with the experimental [9, 10, 49] and theoretical results [50–52]. The present B_0 is slightly different from experimental [49] and theoretical [50] data for cd phase, but the deviation is acceptable. For dhcp and fcc phases, definite experimental information about the equilibrium properties was unavailable, based on the fact that the structure of dhcp phase had not been identified at 38–42 GPa. Also, crystallographic measurement of the fcc phase above 70 GPa is difficult. By taking into account the influence of pressure, a separate plot of the change in volume versus pressure for these six phases of Si at the ground state is presented in Fig. 2b. Compared to the previous calculation [53], it is shown that the present results are consistent with those calculated by Malone et al. [53].

Phonon dispersion

Theoretically, the phonon spectrum, as well as the corresponding phDOS at certain pressures, can be obtained by the calculation at corresponding

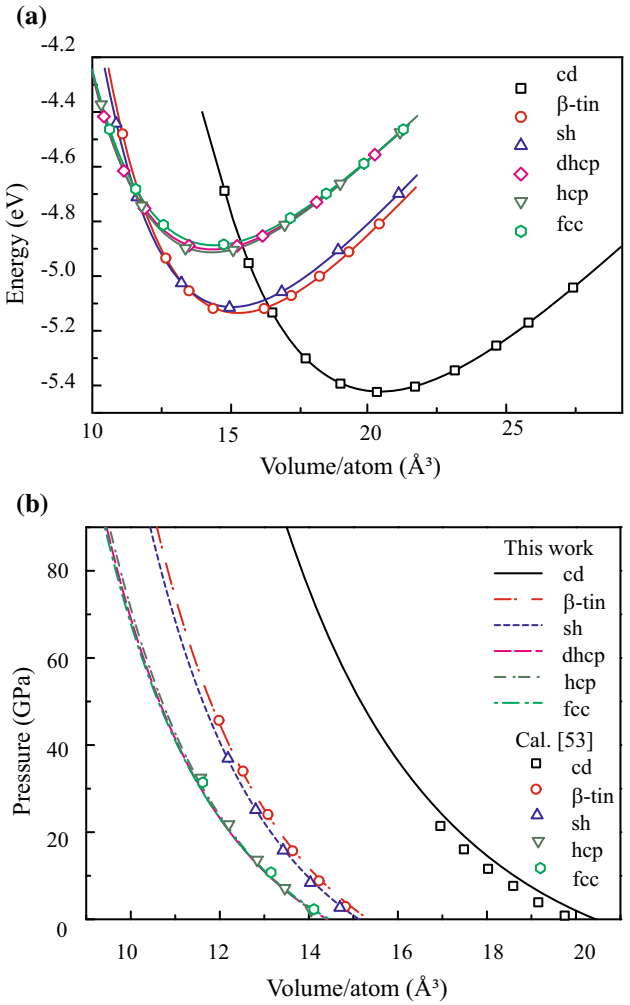

Figure 2 Total energy of six structures of Si as a function of volume per atom. Open symbols are direct calculation results. Solid lines are fitted E–V curves according to the third-order B-M EOS. **b** Pressure as a function of volume per atom of six structures compared with calculated data from Ref. [53].

volumes. The calculated phonon dispersion curves and phDOS for cd, β-tin and sh phases are presented in Fig. 3. The volume and temperature values were chosen according to the experimental and theoretical conditions. The experimental data [54, 55] of cd phase from inelastic neutron-scattering measurement [56] and the previous calculations [57, 58] for β-tin and sh phases are included for comparison. Figure 3a shows the phonon dispersion of the cd phase along the L–Γ–K–X–W–L–K–X–W–Γ directions. The segments Γ–X, Γ–K and Γ–L are, respectively, along the [00ζ], [ζζ0] and [ζζζ]. It is clear that these results of cd phase are in good agreement with the experimental data [54, 55], which seems better than some of the

Table 1 Calculated lattice constants a and c (Å), atomic volume V_0 (Å^3/atom), bulk modulus B_0 (GPa), bulk modulus pressure derivative B_0' and static energy E_0 (eV) for six phases of Si

Phase	Space group	a	c/a	V_0	B_0	B_0'	E_0	References
cd	Fd-3 ms	5.468		20.446	87	4.364	− 43.378	This work
		5.435		20.068	98	4.240		Exp. [49]
					98			Cal. [50]
β-tin	I41/amdS	4.753	0.539	14.469	104	4.482	− 20.540	This work
		4.690	0.550	14.185				Exp. [9]
		4.705	0.550	14.321				Cal. [50]
		4.691	0.525	13.553	119	4.010		Cal. [52]
		4.565	0.551	13.104				Cal. [51]
sh	P6/mmm	2.538	0.948	13.422	103	4.539	− 5.113	This work
		2.551	0.941	13.450				Exp. [9]
		2.527	0.937	13.120				Exp. [10]
		2.400	0.957	13.227	106	4.860		Cal. [52]
		2.561	0.955	13.500				Cal. [51]
dhcp	P63 mc	2.737	3.250	57.623	85	4.313	− 19.611	This work
hcp	P63/mmc	2.527	1.601	11.187	88	4.345	− 9.827	This work
		2.524	1.640	11.419				Exp. [9]
		2.444	1.700	10.746				Exp. [10]
		2.469	1.695	11.047				Cal. [51]
fcc	Fm-3m	3.405		9.869	83	4.211	− 19.549	This work

For comparison, experimental data and previous calculated results are also listed

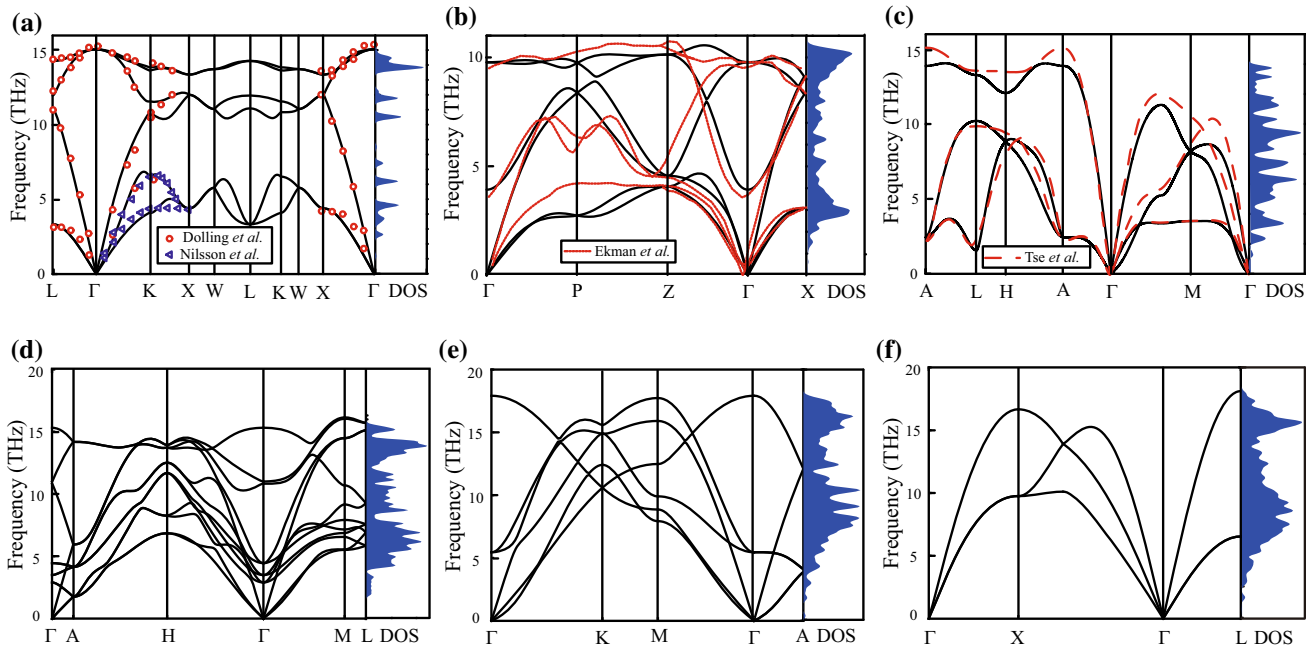

Figure 3 Phonon dispersion curves are plotted as solid lines for **a** the cd structure at volume 20.02 Å^3/atom, **b** the β-tin structure at volume 15.36 Å3/atom, **c** the sh structure at volume 13.31 Å^3/atom, **d** the dhcp structure at volume 11.235 Å^3/atom, **e** the hcp structure at volume 9.74 Å^3/atom and **f** the fcc structure at volume 9.83 Å^3/atom. The present phonon results of the cd structure are compared with the experimental data from Refs. [54, 55], and the results of the β-tin and sh structures are compared with the calculated data from Refs. [57, 58], respectively.

theoretical values [59–61]. In Fig. 3b, c, the phonon dispersions of β-tin and sh phases are shown, which are along several high-symmetry directions (Γ–P–Z–Γ–X and A–L–H–A–Γ–M–Γ, respectively) in the Brillouin zone. The high-symmetry points here correspond to Γ $(0,0,0)$, P $(\frac{1}{4},\frac{1}{4},\frac{1}{4})$, Z $(-\frac{1}{2},\frac{1}{2},\frac{1}{2})$, X

$(0,0,\frac{1}{2})$, A $(0,0,\frac{1}{2})$, L $(0,\frac{1}{2},\frac{1}{2})$, H $(-\frac{1}{3},\frac{2}{3},\frac{1}{2})$ and M $(0,\frac{1}{2},0)$. It should be noted that a similar comparison is found for β-tin and sh phases, with accurate agreement at relatively low frequencies and slight discrepancies at high frequencies (respectively), compared with the findings of previous calculations [57, 58]. Explicitly, the optical modes of the β-tin and sh phases at high frequencies are marginally higher than the previous results calculated by Ekman et al. [57] and John et al. [58], respectively. In view of the reasonableness of the present results, well-tested parameters were used to investigate the phonon spectra of the other three phases under the conditions of high pressure. The findings are shown in Fig. 3d–f. For these three high-pressure phases (dhcp, hcp and fcc), there was not yet any experimental phonon data to compare. In general, as there are no negative frequencies in the phonon dispersion curves, the six structures are mechanically stable at corresponding volumes or pressures. The results then were used to deduce the thermodynamic properties of these phases.

Thermodynamic properties

By integrating the phDOS, the thermodynamic properties of each phase, in terms of their volumetric expansion coefficient (α), heat capacity at constant pressure (C_P), entropy (S) and Helmholtz free energy (F), can be obtained as a function of temperature or pressure. The temperature dependence of α for these six phases is presented in Fig. 4, where the experimental data [62–66] of the cd phase are included. It can be observed that the evolution of α for the cd phase is very consistent with the calculated and experimental results. In particular, the locations of the minimum at $-2.03\times10^{-6}\ K^{-1}$ at 100 K for calculation and $-1.42\times10^{-6}\ K^{-1}$ for experiments [62, 63] almost coincide, and both of which exhibit the feature of negative thermal expansion. In general, it is believed that the unusual negative thermal expansion behavior can be ascribed to the negative Grüeisen parameter (γ_{th}) of the transverse acoustic (TA) phonons near the Brillouin zone boundary [67, 68]. The origin of the negative γ_{th} is that phonon frequency increases as crystal volume increases. In contrast to cd phase, the feature of negative thermal expansion is not really found in the β-tin phase. Straightforwardly, our results of α for the β-tin phase agree well with the

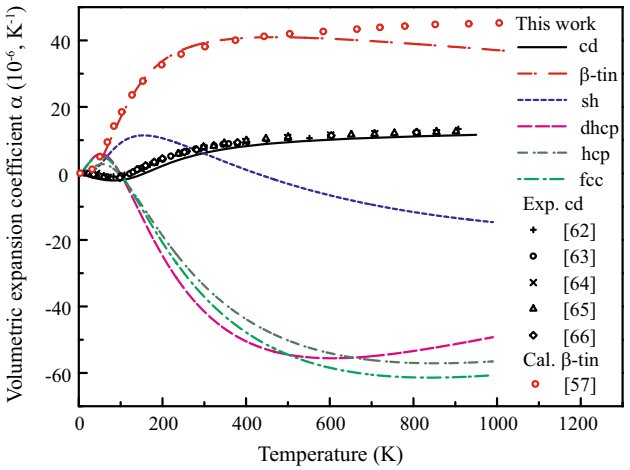

Figure 4 Volumetric expansion coefficient (α) of six structures of Si as a function of temperature. The experimental data of the cd structure and theoretical data of the β-tin structure are plotted as symbols from Ref. [63–67] and [57], respectively.

previous calculation [57] for the temperature range of 0–600 K, but a slight difference is evident above 600 K and the difference will continue to increase at higher temperatures. The α components of other four phases perform similarly in that the same trend of initial α increase and then a subsequent decrease to very negative values. Figure 5 shows the temperature dependence of heat capacity C_P's of cd-, β-tin-, sh-, dhcp-, hcp- and fcc-Si at ambient pressure. The experimental data [69] of the cd phase are included for comparison. It is apparent that the present results for the cd phase mirror well the experimental values

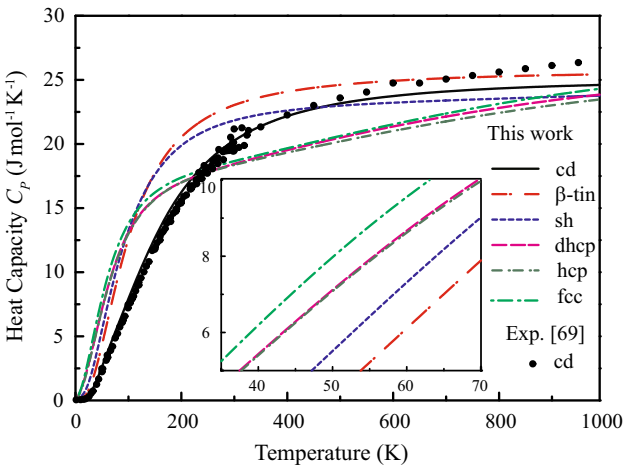

Figure 5 Heat capacity at constant pressure (C_P) of six structures of Si as a function of temperature. The inset shows the enlarged C_P of each phase ranging from about 35 to 70 K. The experimental data of the cd structure are plotted as solid circles from Ref. [62].

[69] although slight differences exist above 600 K. Specifically, the calculated C_P of the cd phase (20.28 J mol^{-1} K^{-1}) is very close to the experimental data (20.06 J mol^{-1} K^{-1}) at ambient conditions. By comparison, the C_P's of the fcc phase are larger than those of other phases at low temperatures, while in the high-temperature region, the highest C_P is in turn found in the β-tin phase. In the present work, the C_P was evaluated using the thermodynamic relationship between C_V and C_P such as $C_P = C_V + \alpha^2 B_T V T$. In the high-temperature region, the phDOS is of great importance to the C_V. The highest phDOS of the β-tin phase brings about the highest C_P in the high-temperature region. In Figs. 6 and 7, the S and F of each phase as a function of temperature are displayed, respectively. As is evident, the calculated values of S for the cd phase in the present study are very close to the experimental values [70]. Moreover, the S and F values of the cd phase are the lowest at any temperature, meaning that the cd phase can be stable at any temperature at atmospheric pressure.

Pressure–temperature phase diagram

Phase transition behavior can be accessed by rule of the Gibbs energy as a function of pressure and temperature $G(T,P) = F(T,V) + PV$. Under specified conditions of pressure and temperature, F is described by the contributions of E_{sta}, F_{vib}, F_{ele} and F_{zp} that have been introduced above in "Theory" section. Figure 8a shows the calculated values of G for

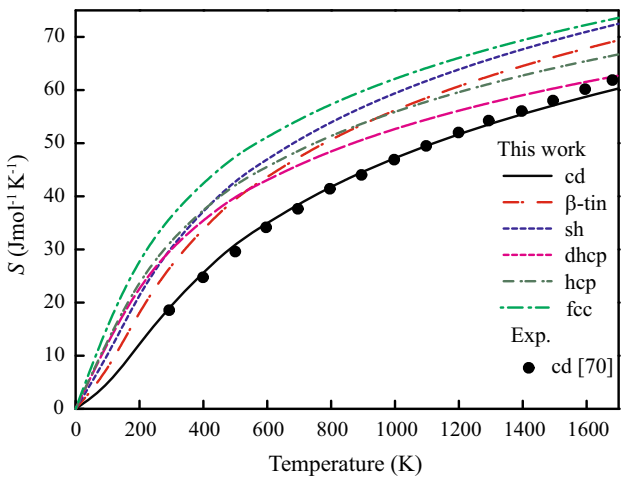

Figure 6 Entropy (S) of six structures of Si as a function of temperature. The experimental data of the cd structure from Ref. [70] are plotted as solid circles.

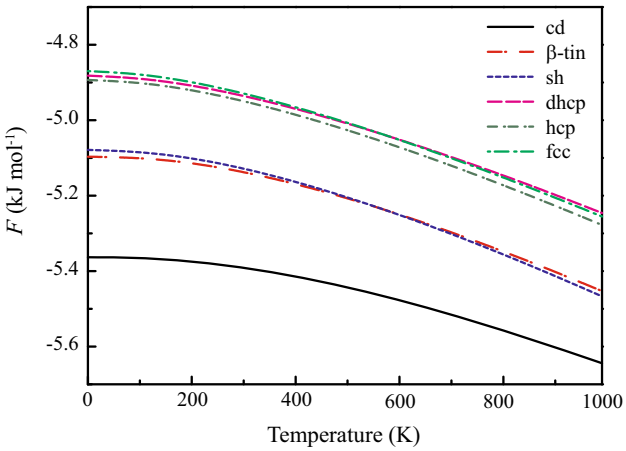

Figure 7 Helmholtz free energy (F) of six structures of Si as a function of temperature.

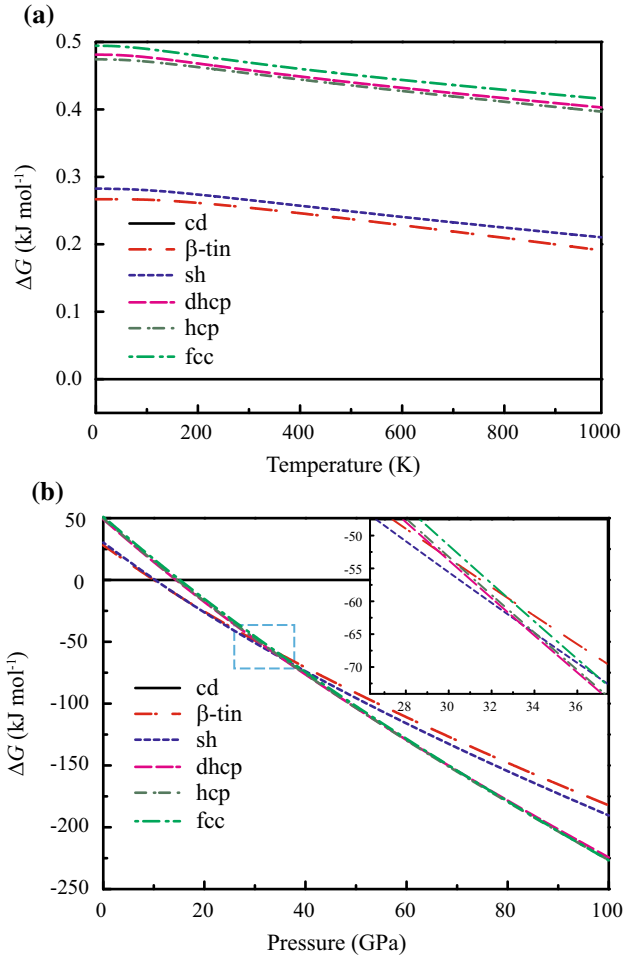

Figure 8 Gibbs free energy (G) of six phases as function of **a** temperature at 0 GPa and **b** pressure at 300 K, taking that of the cd structure as reference. The inset shows an enlarged picture of region marked by the blue dash line.

these six phases as a function of temperature at 0 GPa. The cd phase has the lowest G within the whole temperature range, which indicates that cd is the preferred phase, compared to other phases, at 0 GPa. The situation is dramatically different, however, when there is external pressure, as shown in Fig. 8b. As indicated in Fig. 8b, the relative stability of the cd phase in comparison with other phases is gradually changed by pressure at 300 K. In consequence, the G's for those phases have crossover points, located at about 11, 14 and 33 GPa, from which the phase transition pressure can be determined, i.e., cd → β-tin → sh → dhcp at 11, 14 and 33 GPa, respectively. The predicted transition pressures are consistent with the experimental [4, 5, 9, 11, 24, 27, 71, 72] and calculated [15, 16, 26, 31, 51] results. In the high-pressure region, the crossover points of the G's for the rest of phases are not visually differentiable. It indicates that the stabilities of these phases are close to each other at 300 K. To figure out the phase relationship of dhcp, hcp and fcc at high pressure, the phase diagram must be addressed.

By complying with the principle of minimum free energy as a function of temperature and pressure, the phase transition points in the entire phase space can be determined, as depicted in Fig. 9. The available experimental data and calculated points also are included. The phase transitions (cd → β-tin → sh → dhcp → hcp → fcc) occur in sequence along with increasing pressure at room temperature. In the low-pressure region, the cd phase is

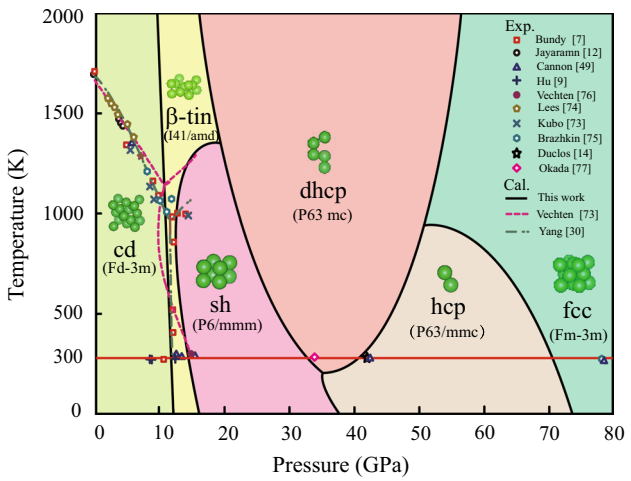

Figure 9 Calculated P–T phase diagram of Si (indicated by solid lines) compared with selected experimental and theoretical results.

stable until the pressure reaches 11 GPa, at which point the phase transition of cd → β-tin would take place. Numerically, the phase transition line for cd → β-tin is about a vertical line with $dP/dT \approx -0.003$ GPa K^{-1}, which belongs to the range of experimental results (− 0.065 to 0.002 GPa K^{-1}) [49]. In addition, the present slope of transition line for cd → β-tin is very close to the value (− 0.00058 GPa K^{-1}) reported by previous calculation [30]. The melting points of the cd phase were drawn according to the available experimental data [73–75]. At room temperature, the phase transition (β-tin → sh) is predicted to occur at about 14 GPa, which is in an excellent agreement with the experimental data (13–16 GPa). When temperature is above 1350 K, the β-tin phase transits directly to the dhcp phase at about 19 GPa. Therefore, the three-phase (β-tin, sh, dhcp) coexistence point (19 GPa, 1400 K) can be determined. By comparison, the phase boundary between β-tin and sh calculated by this work for high temperature is even higher than the melting points of β-tin calculated by Vechten et al. [76] and Yang et al. [30]. In the calculations by Yang et al. [30], the Clapeyron equation, $dP = \frac{\Delta H(T)}{\Delta V(P)T} dT$, was employed to evaluate the thermodynamic properties, though with the semiempirical model and approximate values of parameters. Thus, the estimated pressure-dependent melting points might deviate significantly from their true values. In the present work, the thermodynamic parameters were, by contrast, obtained on the basis of the physical analytic model, in which the parameters were generated by ab initio calculations. In this scenario, the melting point of the β-tin phase is supposed to be higher than that predicted by Yang et al. [30]. At room temperature, the phase transition of sh → dhcp would occur at 33 GPa, which is very close to the experimental data 34 GPa [77]. Furthermore, the sh-dhcp coexistence line has a large negative pressure derivative, which decreases slightly toward smaller negative values as the pressure increases. Additionally, when temperature is below 230 K, it is worth noticing that the sh phase transforms into the hcp phase. This transitional tendency results in the presence of a triple point (sh, dhcp, hcp) at 35 GPa and 230 K. Unfortunately, in the high-temperature range, no other experimental data or calculations were available to provide confirmation of the predicted phase transition behavior. When the pressure reaches about 41 GPa, hcp becomes the

stable phase at room temperature. The transitional pressure is in a good agreement with test results [10, 13]. As the pressure is further increased, the calculations predict that the hcp phase would, in turn, transform to a fcc phase at 72 GPa, which is slightly lower than the measured experimental data of 79 GPa [11, 13, 14]. This underestimation is attributed to a simplification of the model used by this work, in which defects and impurities are not taken into account. The pressure-dependent transition of the fcc phase also is affected by temperature, i.e., hcp → fcc at temperatures below 950 K and dhcp → fcc at temperatures above 950 K. Consequently, a triple point in terms of dhcp, hcp and fcc phases is located at (52 GPa, 950 K). At the limits of high pressure and high temperature in the current phase diagram, the fcc phase is extremely stable. This is consistent with the previous prediction that fcc phase can be stable up to 248 GPa [13].

Conclusions

The first-principles method has been employed to predict the high-pressure–temperature phase diagram of Si for a wide range of pressures and temperatures from 0 to 80 GPa and 0 to 2000 K, respectively. The thermodynamic quantities of six phases (cd, β-tin, sh, dhcp, hcp and fcc) were taken into consideration. It is confirmed that the predicted thermodynamic properties and relevant phase transitions of Si at low pressures or temperatures are very consistent with previous experimental results and calculated data. In this framework, the critical phase transitions of the cd, β-tin, sh, dhcp, hcp and fcc under the conditions of high pressure and temperature are successfully predicted. The critical phase transitions are cd → β-tin → sh → dhcp → hcp → fcc, whose transitional pressures are 11, 14, 33, 41 and 72 GPa at room temperature, respectively. In particular, three triple points were determined at (19 GPa, 1400 K) of the β-tin, sh and dhcp phases, (35 GPa, 230 K) of the sh, dhcp and hcp phases, and (52 GPa, 950 K) of the dhcp, hcp and fcc phases, respectively.

Acknowledgements

This work was supported by the National Natural Science Foundation of China (Grant Nos. 51571168 and 51601160), the National Key R&D Program of China (Grant No. 2017YFB0702901), the Ministry of Science and Technology of China (Grant No. 2014DFA53040) and the Natural Science Foundation of Fujian Province, China (No. 2016J05133).

Compliance with ethical standards

Conflict of interest The authors declare that they have no competing interests.

References

[1] Kodiyalam S, Kalia RK, Kikuchi H, Nakano A, Shimojo F, Vashishta P (2001) Grain boundaries in gallium arsenide nanocrystals under pressure: a parallel molecular-dynamics study. Phys Rev Lett 86:55–58

[2] Malone BD, Louie SG, Cohen ML (2010) Electronic and optical properties of body-centered-tetragonal Si and Ge. Phys Rev B 81:115201

[3] Georg RB, Halliday AN, Schauble EA, Reynolds BC (2007) Silicon in the earth's core. Nature 447:1102–1106

[4] Hanflan M, Schwarz U, Syassen K, Takemura K (1999) Crystal structure of the high-pressure phase silicon VI. Phys Rev Lett 82:1197–1200

[5] Minomura S, Drickamer HG (1962) Pressure induced phase transitions in Silicon, Germanium and some III–V compounds. J Phys Chem Solids 23:451–456

[6] Jamieson JC (1963) Crystal structures at high pressures of metallic modifications of silicon and germanium. Science 139:762–764

[7] Bundy FP (1964) Phase diagrams of Silicon and Germanium to 200 kbar, 1000 C. J Chem Phys 41:3809–3814

[8] Welber B, Kim CK, Cardona M, Rodriguez S (1975) Dependence of the indirect energy gap of silicon on hydrostatic pressure. Solid State Commun 17:1021–1024

[9] Hu JZ, Merkle LD, Menoni CS, Spain IL (1986) Crystal data for high-pressure phases of silicon. Phys Rev B 34:4679–4684

[10] Olijnyk H, Sikka SK, Holzapfel WB (1984) Structural phase transitions in Si and Ge under pressures up to 50 GPa. Phys Lett A 103:137–140

[11] Hu JZ, Spain IL (1984) Phases of silicon at high pressure. Solid State Commun 51:263–266

[12] Jayaraman A, Klement W, Kennedy GC (1963) Melting and polymorphism at high pressures in some group IV elements and III–V compounds with the diamond/zincblende structure. Phys Rev 130:540–547

[13] Duclos SJ, Vohra YK, Ruoff AL (1990) Experimental study of the crystal stability and equation of state of Si to 248 GPa. Phys Rev B 41:12021–12028

[14] Duclos SJ, Vohra YK, Ruoff AL (1987) Hcp to fcc transition in Silicon at 78 GPa and studies to 100 GPa. Phys Rev Lett 58:775–777

[15] Ahuja R, Eriksson O, Johansson B (1999) Theoretical high-pressure studies of silicon VI. Phys Rev B Condens Matter Mater Phys 60:475–477

[16] Needs RJ, Mujica A (1995) A first-principles pseudopotential dtudy of the structural phases of Silicon. Phys Rev B 51:9652–9660

[17] Kasper JS, Richards SM (1964) The crystal structures of new forms of silicon and germanium. Acta Cryst 17:752–755

[18] Besson JM, Mokhtari EH, Gonzalez J, Weill G (1987) Electrical properties of demimetallic silicon III and semiconductive silicon IV at ambient pressure. Phys Rev Lett 59:473–476

[19] Zhao YX, Buehler F, Sites JR, Spain IL (1986) New metastable phases of Silicon. Solid State Commun 59:679–682

[20] Piltz RO, Maclean JR, Clark SJ, Ackland GJ, Hatton PD, Crain J (1995) Structure and properties of silicon XII: a complex tetrahedrally bonded phase. Phys Rev B 52:4072–4085

[21] Crain J, Ackland GJ, Maclean JR, Piltz RO, Hatton PD, Pawley GS (1994) Reversible pressure-induced structural transitions between metastable phases of silicon. Phys Rev B 50:13043–13046

[22] Pfrommer BG, Côté M, Louie SG, Cohen ML (1997) Ab initio study of Silicon in the R8 phase. Phys Rev B 56:6662–6668

[23] Nguyen MC, Zhao X, Wang Y, Wang CZ, Ho KM (2014) Genetic algorithm prediction of crystal structure of metastable Si-IX phase. Solid State Commun 182:14–16

[24] Goettel KA, Mao HK, Bell PM (1985) Generation of static pressures above 2.5 megabars in a diamond-anvil pressure cell. Rev Sci Instrum 56:1420–1427

[25] Domnich V, Gogotsi Y (2002) Phase transformations in Silicon under contact loading. Rev Adv Mater Sci 3:1–36

[26] Broughton JQ, Li XP (1987) Phase diagram of silicon by molecular dynamics. Phys Rev B 35:9120–9127

[27] Hebbache M, Mattesini M, Szeftel J (2001) Pressure-induced structural sequence in silicon: diamond to β-Tin to imma. Phys Rev B 63:205201

[28] Yang CC, Li JC, Jiang Q (2003) Effect of pressure on melting temperature of silicon determined by Clapeyron equation. Chem Phys Lett 372:156–159

[29] Gaál-Nagy K, Bauer A, Pavone P, Strauch D (2004) Ab initio study of the enthalpy barriers of the high-pressure phase transition from the cubic-diamond to the β-Tin structure of Silicon and Germanium. Comput Mater Sci 30:1–7

[30] Yang CC, Li JC, Jiang Q (2004) Temperature-pressure phase diagram of silicon determined by Clapeyron equation. Solid State Commun 129:437–441

[31] Kaczmarski M, Bedoya-Martinez ON, Hernandez ER (2005) Phase diagram of silicon from atomistic simulations. Phys Rev Lett 94:095701

[32] Wang CP, Li C, Han JJ, Yan LH, Deng B, Liu XJ (2017) The pressure-temperature phase diagram of pure Co based on first-principles calculations. Phys Chem Chem Phys 19:22061–22068

[33] Mei ZG, Shang SL, Wang Y, Liu ZK (2009) Density-functional study of the thermodynamic properties and the pressure-temperature phase diagram of Ti. Phys Rev B 80:104116

[34] Lee C, Gonze X (1995) Ab initio calculation of the thermodynamic properties and atomic temperature factors of SiO_2 α-quartz and stishovite. Phys Rev B 51:8610–8613

[35] Mermin ND (1965) Thermal properties of the inhomogeneous electron gas. Phys Rev 137:A1441–A1443

[36] Kresse G (1998) From ultrasoft pseudopotentials to the projector augmented-wave method. Phys Rev B 59:1758–1775

[37] Kresse G, Furthmüller J (1996) Efficiency of ab initio total energy calculations for metals and semiconductors using a plane-wave basis set. Comput Mater Sci 6:15–50

[38] Perdew J, Burke K, Ernzerhof M (1996) K^+ emission in symmetric heavy ion reactions at subthreshold energies. Phys Rev Lett 78:1396

[39] Blöchl PE (1994) Projector augmented-wave method. Phys Rev B 50:17953–17979

[40] Monkhorst HJ, Pack JD (1976) Special points for Brillouin-zone integrations. Phys Rev B 13:5188–5192

[41] Baroni S, Gironcoli SD, Corso AD, Giannozzi P (2001) Phonons and related crystal properties from density-functional. Rev Mod Phys 73:515–562

[42] Togo A, Oba F, Tanaka I (2008) First-principles calculations of the ferroelastic transition between rutile-type and $CaCl_2$-type SiO_2 at high pressures. Phys Rev B 78:134106

[43] Togo A, Chaput L, Tanaka I, Hug G (2010) First-principles phonon calculations of thermal expansion in Ti_3SiC_2, Ti_3AlC_2, and Ti_3GeC_2. Phys Rev B 81:174301

[44] Liu ZL (2015) Phasego: a toolkit for automatic calculation and plot of phase diagram. Comput Phys Commun 191:150–158

[45] Liu ZL (2015) Phasego 2.0: counting full anharmonic effects from high-temperature phonon density of states. Comput Phys Commun 197:341–342

[46] Liu ZL, Wang HY, Li XF (2016) Phasego 3.0: automatic analysis of synthesis and decomposition. Comput Phys Commun 29:197–198

[47] Birch F (1978) Finite strain isotherm and velocities for single-crystal and polycrystalline NaCl at high pressures and 300 K. J Geophys Res Solid Earth 83:1257–1268

[48] Baonza VG, Cáceres M, Núñez J (1995) Universal compressibility behavior of dense phases. Phys Rev B 51:28–37
[49] Cannon JF (1974) Behavior of the elements at high pressures. J Phys Chem Ref Data 3:781–824
[50] Yin MT, Cohen ML (1984) Structural theory of graphite and graphitic silicon. Phys Rev B 29:6996–6998
[51] Chang KJ, Cohen ML (1985) Solid-solid phase transitions and soft phonon modes in highly condensed Si. Phys Rev B 31:7819–7826
[52] Needs RJ, Martin RM (1984) Transition from β-tin to simple hexagonal Silicon under pressure. Phys Rev B 30:5390–5392
[53] Malone BD, Cohen ML (2012) Prediction of a metastable phase of Silicon in the Ibam structure. Phys Rev B 85:024116
[54] Nilsson G, Nelin G (1972) Study of the homology between silicon and germanium by thermal-neutron spectrometry. Phys Rev B 6:3777–3786
[55] Dolling G, Cowley RA (1966) The thermodynamic and optical properties of germanium, silicon, diamond and gallium. Proc Phys Soc 88:463–494
[56] Wakabayashi N, Scherm RH, Smith HG (1982) Lattice dynamic of Ti Co, Tc, and other hcp transition metals. Phys Rev B 25:5122–5132
[57] Ekman M, Persson K, Grimvall G (2000) Lattice dynamics and thermodynamic properties of the β-Sn phase in Si. Phys Rev B 62:14784–14789
[58] Tse JS, Klug DD, Patchkovskii S, Ma Y, Dewhurst JK (2006) Chemical bonding, electron-phonon coupling, and structural transformations in high-pressure phases of Si. J Phys Chem B 110:3721–3726
[59] Giannozzi P, de Gironcoli S, Pavone P, Baroni S (1991) Ab initio calculation of phonon dispersions in semiconductors. Phys Rev B 43:7231–7242
[60] Wei S, Chou MY (1994) Phonon dispersions of silicon and germanium from first-principles calculations. Phys Rev B 50:2221–2226
[61] Favot F, Corso AD (1999) Phonon dispersions performance of the generalized gradient approximation. Phys Rev B 60:11427
[62] Carr RH, McCammon RD, White GK (1965) Thermal expansion of germanium and silicon at low temperatures. Philos Mag 12:157–163
[63] Ibach H (1969) Thermal expansion of Silicon and Zinc Oxide. Phys Stat Solid 31:625–634
[64] Yim WM, Paff RJ (1974) Thermal expansion of AlN, sapphire, and silicon. J Appl Phys 45:1456–1457
[65] Roberts RB (1981) Thermal expansion reference data Silicon 300–850 K. J Phys D Appl Phys 14:163–166
[66] Lyon KG, Salinger GL, Swenson CA, White GK (1977) Linear thermal expansion measurements on Silicon from 6 to 340 K. J Appl Phys 48:865–868
[67] Xu CH, Wang CZ, Chan CT, Ho KM (1991) Theory of the thermal expansion of Si and diamond. Phys Rev B 43:5024–5027
[68] Yin MT, Cohen ML (1980) Theory of the phase transformation and lattice dynamics of Si. Phys Rev Lett 45:1004–1007
[69] Flubacher P, Leadbetter AJ, Morrison JA (1959) The heat capacity of pure silicon and germanium and properties of their vibrational frequency spectra. Philos Mag 4:273–294
[70] Chase MW, Davies CA, Downey JR, Frurip DJ, Mcdonald RA, Syverud AN (1985) Janaf thermochemical table. J Phys Chem Ref Data 14:1–926
[71] Sharma SM, Sikka SK (1985) Lattice dynamical analysis of β-γ phase transformation in Silicon under high pressure. J Phys Chem Solids 46:477–479
[72] Voronin GA, Pantea C, Zerda TW, Wang L, Zhao Y (2003) In situx-ray diffraction study of Silicon at pressures up to 15.5 GPa and temperatures up to 1073 K. Phys Rev B 68:020102
[73] Kubo A, Wang Y, Runge CE, Uchida T, Kiefer B, Nishiyama N, Duffy TS (2008) Melting curve of silicon to 15 GPa determined by two-dimensional angle-dispersive diffraction using a kawai-type apparatus with x-ray transparent sintered diamond anvils. J Phys Chem Solids 69:2255–2260
[74] Lees J, Williamson BHJ (1965) Combined very high pressure high temperature calibration of the tetrahedral anvil apparatus, fusion curves of zinc, aluminium, germanium and silicon to 60 kilobars. Nature 208:278–279
[75] Brazhkin VV, Lyapin AG, Popova SV, Voloshin RN (1995) Nonequilibrium phase transitions and amorphization in Si, Si/Gaas, Ge, and Ge/Gasb at the decompression of high-pressure phases. Phys Rev B 51:7549–7554
[76] Vechten JAV (1973) Quantum dielectric theory of electronegativity in covalent systems. III. Pressure-temperature phase diagrams, heats of mixing, and distribution coefficients. Phys Rev B 7:1479–1507
[77] Okada Y, Tokumaru Y (1984) Precise determination of lattice parameter and thermal expansion coefficient of silicon between 300 and 1500 K. J Appl Phys 56:314–320